On the effect of yttrium promotion on Ni-layered double hydroxides-derived catalysts for hydrogenation of CO2 to methane

Chao Sun, Katarzyna Świrk, Dominik Wierzbicki, Monika Motak, Teresa Grzybek, Patrick da Costa

On the effect of yttrium promotion on Ni- layered double hydroxides-derived catalysts for hydrogenation of CO_2 to methane

Chao Sun [a], Katarzyna Świrk [a, b], Dominik Wierzbicki [a, b], Monika Motak [b], Teresa Grzybek [b],

Patrick Da Costa [a,*]

[a] Sorbonne Université, CNRS UMR 7190, Institut Jean Le Rond d'Alembert, 2 Place de la Gare de Ceinture, 78210 Saint-Cyr-L'École, France

[b] AGH University of Science and Technology, Faculty of Energy and Fuels, Al. A. Mickiewicza 30, 30-059 Cracow, Poland

* patrick.da_costa@sorbonne-universite.fr; chao.sun@dalembert.upmc.fr

Abstract:

Ni-containing mixed oxides derived from layered double hydroxides with various amounts of yttrium were synthesized by a co-precipitation method at constant pH and then obtained by thermal decomposition. The characterization techniques of XRD, elemental analysis, low-temperature N_2 sorption, H_2-TPR, CO_2-TPD, TGA and TPO were used on the studied catalysts. The catalytic activity of the catalysts was evaluated in the CO_2 methanation reaction performed at atmospheric pressure. The obtained results confirmed the formation of nano-sized mixed oxides after the thermal decomposition of hydrotalcites. The introduction of yttrium to Ni/Mg/Al layered double hydroxides led to a stronger interaction between nickel species and the matrix support and decreased nickel particle size as compared to the yttrium-free catalyst. The modification with Y (0.4 and 2 wt.%) had a positive effect on the catalytic performance in the moderate temperature region (250-300 °C), with CO_2 conversion

increasing from 16 % for MO-0Y to 81% and 40% for MO-0.4Y and MO-2.0Y at 250 °C, respectively. The improved activity may be correlated with the increase of percentage of medium-strength basic sites, the stronger metal-support interaction, as well as decreased crystallite size of metallic nickel. High selectivity towards methane of 99% formation at 250 °C was registered for all the catalysts.

Keywords: CO_2 methanation, hydrotalcite, mixed oxides, yttrium, nickel catalyst

1. Introduction

The reduction of CO_2 emissions has gained legislative importance as it is considered one of the major drivers of climate change [1]. The reduction of carbon dioxide emissions is becoming attractive because of the cost of carbon feedstock [2]. CO_2 hydrogenation into methane over transition metal-based catalysts using renewable hydrogen from water electrolysis as an example has a huge potential to reduce the emissions and, at the same time, to store the excess renewable energy to equalize the demand and capacity in a power to gas process [3–5]. Due to the lack of costly infrastructure for the distribution and storage of hydrogen, CO_2 hydrogenation seems to be a promising alternative approach [6,7]. Additionally, methane can be easily liquefied and stored in the existing infrastructure [7]. Out of all proposed CO_2 hydrogenation reactions, e.g., methanol synthesis, higher hydrocarbons or methanation, the most developed one methanation ($CO_2 + 4H_2 = CH_4 + 2H_2O$), with a few plants already operational in European Union [8,9].

The most widely studied catalysts for Sabatier's reaction in literatures are those based on group 8, 9, 10 metals-Fe, Ru, Rh, Co, Ni, or Pt [3,6,10–22]. However, the most active and selective catalysts towards methane were found to be those based on Rh, Ru and Ni [6,9,10,19,22–24]. Nickel-based catalysts have the advantage over noble metal-based catalysts because of their low cost, high availability and accessibility[7,25–28].

Layered double hydroxides (LDH) or hydrotalcite (HT) are materials with di- and tri-valent cations incorporated into the brucite-like layers. The layers of hydrotalcites are positively charged, and anions present in the interlayer spaces are compensating the charge. It was reported in the literature that there is a wide range of cations that maybe incorporated into the hydrotalcites structure, e.g., Li^{+}, Ti^{4+}, Sn^{4+} or Zr^{4+} [29]. Calcination of such materials leads to the formation of mixed nano-oxides with periclase-like structure, which show very interesting features [7,30–34]. Redox or acid-base properties of such materials may be tailored to some extent by controlling hydrotalcite composition, as shown e.g. in NH_3-SCR [35–39] or DRM [40–45] reactions. Another advantage of double layered hydroxides is that the incorporated cations are usually homogenously distributed due to their random arrangement in the brucite-like layers. Moreover, such materials exhibit basic properties, which are of great interest when used as catalysts for the reaction of CO_2 methanation [35,44,46–51].

Several aspects were already investigated in case of hydrotalcite-derived catalysts for CO_2 methanation reaction such as (i) the effect of nickel content, (ii) the particle

size of nickel crystallites, (iii) the reducibility of nickel species, (iv) the number and distribution of basic sites, and (v) the promotion with other metals such as La, Fe, etc. or the new preparation method[46,49,52–56].

Fan et al. [57] studied Ni impregnated $MgAl_2O_4$ derived from hydrotalcite followed by calcination at 500 °C or treated by DBD plasma in order to decompose Ni precursor. The plasma treatment resulted in higher nickel dispersion of 7.1% for plasma decomposition method prepared sample, compared to 6.0% for the traditionally calcined material. The authors claimed that smaller metallic nickel particles resulted in enhanced activity in the reaction of CO_2 methanation. Wang et al. [55] studied Ni/Al HTs promoted with 0.05 and 0.25% molar ratio of Fe and found that the introduction of Fe effectively enhanced the H_2 adsorption capacity. Ni/Mg/Al hydrotalcites promoted with a wide range of Fe content (1.2-18 wt.% of Fe) were examined by Mebrahtu et al. [58]. It was found that the activity in CO_2 methanation was effectively increased in the low temperature region when low amounts of iron were introduced. In our previous reports, we investigated the influence of Ni loading and the effect of La introduction on the catalytic activity of LDHs catalysts in CO_2 methanation [46,49,50]. The incorporation of higher amounts of nickel, as well as introduction of lanthanum, significantly enhanced the activity in CO_2 methanation reaction. This could be correlated with the increased number of medium-strength basic sites, which in case of La-promoted catalysts was strongly dependent on the method of promoter introduction [49][59][60]. According to the study of Pan et al. [60]

CO_2 adsorbed on $Ni/Ce_{0.5}Zr_{0.5}O_2$ may undergo hydrogenation easier than on Ni/Al_2O_3 because of the higher content of medium basic sites.

Yttrium had been reported in the literature as a promising dopant in methane dry reforming reaction ($CO_2 + CH_4 = 2H_2 + 2CO$) [44,47,61–66]. The increased activity of the Ni-containing hyrotalcites was attributed to the enhanced dispersion of the active phase in comparison with the un-promoted materials [44,47,64]. The stability of the Zr- containing catalysts in DRM reaction was also enhanced by the introduction of Y, which was assigned to the formation of a solid-solution ZrO_2-Y_2O_3, leading to the increased reducibility of bulk NiO [45]. Moreover, Bellido et al. [67] reported that ceria doped with yttrium showed enhanced oxygen mobility and oxygen vacancies. For CO_2 methanation, Muroyama et al. [68] reported that Y_2O_3 impregnated with Ni revealed very high activity in the low-temperature region in CO_2 methanation when compared to Ni supported on Al_2O_3, ZrO_2 and CeO_2 catalysts. It was attributed to the promoted decomposition of formate species formed during the reaction over Ni/Y_2O_3 catalysts.

To the best of our knowledge, there are no literature reports regarding yttrium promoted Ni-containing hydrotalcite-derived catalysts for CO_2 hydrogenation to methane. Our study was focused on the determination of the influence of Y introduction to Ni-containing layered double hydroxides on the catalytic performance in CO_2 methanation. The catalysts were synthesized using the co-precipitation method at a constant pH and with a fixed molar ratio of M^{II+}/M^{III+} =3.0. The assumed loading of yttrium introduced into hydrotalcite was 0.4, 2.0 and 4.0 wt.%. To correlate the

changes in activity with the Physico-chemical properties, the studied materials were characterized using various techniques such as X-ray diffraction (XRD), low-temperature N_2 sorption, X-ray fluorescence (XRF), temperature-programmed reduction in H_2 (H_2-TPR), temperature-programmed desorption of CO_2 (CO_2-TPD), thermogravimetric analysis (TGA) and temperature-programmed oxidation (TPO).

2. Experimental

2.1. Catalysts preparation

The co-precipitation method with sodium carbonate was carried out for catalyst preparation. An aqueous solution of following nitrates was used: Ni, Y, Al, and Mg, and added dropwise into Na_2CO_3 solution. NaOH (2 M) was also dripped into the mixture to adjust pH to 10±0.2. The ratio of M^{2+}/M^{3+} was assumed as 3. The assumed loading of yttrium was 0.4 wt.%, 2.0 wt.% or 4.0 wt.%. After co-precipitation, the slurry was left to react at 65 ºC for 24 h. Then, this mixture was filtered under vacuum and washed with distilled water. After filtration, the obtained cake was dried at 80 °C overnight and calcined in static air at 550 °C for 5 h with a ramp of 5 °C/min. The samples were designated as MO-0Y, MO-0.4Y, MO-2.0Y, and MO-4.0Y.

2.2. Catalysts characterization

2.2.1. Elemental composition, structural parameters, and textural properties

X-Ray Fluorescence (XRF) using a Rigaku Supermini200 analyzer to evaluate the elemental analysis of the studied catalysts. The experiment was performed under

vacuum at 36.5 ºC in the presence of P-10 gas (a mixture of 10% CH_4/Ar, flow 24.7 mL/min). A pulse height analyzer was used to calibrate the proportional counter (PC) detector. The calcined sample was homogeneously mixed with boric acid and pelletized under 10 bar. So prepared pellet was then covered by polypropylene film (6 μm) and put into a sample holder for the analysis.

The structural properties of the reduced and spent catalysts were studied by X-ray diffraction (XRD). XRD patterns were collected on a PANalytical-Empyrean diffractometer, equipped with a copper-based anode (Cu-Kα, λ = 0.154059 nm). The instrument settings were 40 mA and 45 kV. For the evaluation of Ni^0 (metallic nickel) particle size, the Scherrer equation was used.

Low-temperature N_2 adsorption-desorption method was conducted in a TriStar II 3020 (Micromeritics) apparatus for the study of the textural properties of the catalysts. Before the measurement, 100 mg of the sample was degassed at 110 ºC for 3 h. Then the measurement was carried out at liquid nitrogen temperature (-196 ºC). The specific surface area of the sample was calculated by the Brunauer-Emmett-Teller (BET) method, and the mesopore volume and average pore diameter by the Barrett-Joyner-Halenda (BJH) desorption method.

2.2.2. Temperature programmed reduction in H_2

The reducibility of the hydrotalcite-derived mixed-oxide was measured by temperature-programmed reduction of H_2 (H_2-TPR) method, using a BELCAT-M apparatus (BEL Japan Inc.) equipped with a thermal conductivity detector (TCD). 60

mg of sample was previously degassed in a flow of helium (99.999% He, 50 mL/min) at 100 ºC for 2 h to eliminate impurities, then the sample was reduced from 100 ºC to 900 ºC with the temperature ramp of 10 ºC/min in a 5%H_2/Ar gas mixture (50 mL/min).

2.2.3. Temperature programmed desorption of CO_2

The number and distribution of basic sites were determined by temperature-programmed desorption of CO_2, measured in the same equipment as H_2-TPR. After the TPR experiment, the sample was cooled down to 80 ºC for the TPD test. The sample was pretreated using a flow of pure helium (50 mL/min) at 80 ºC for 2 h, and then CO_2 was adsorbed from 10% CO_2/He mixture (50 mL/min) for 1 h. Then, the catalyst was cleaned by pure helium for 15 min to desorb weakly physically adsorbed CO_2. Afterward, the catalyst was heated from 80 ºC to 800 ºC in He (50 mL/min) with a heating rate of 10 ºC/min. The obtained profiles were deconvoluted and integrated as presented elsewhere [8,9].

2.2.4. Thermogravimetric analyses (TGA)

Thermogravimetric analysis was performed on the spent catalysts by the Q5000 IR apparatus. Around 25 mg of material was heated starting from room temperature to 750 °C (heating rate of 10 °C/min). The measurements were performed in synthetic air. The amount of H_2O and adsorbed CO_2 were estimated by the mass loss registered in the TGA plots.

2.2.5. Temperature-programmed oxidation (TPO)

The TPO analyses were carried out on the spent catalysts by Quadstar Mass equipped with a Pfeiffer Vacuum. Around 30 mg of a sample was heated from ambient temperature to 800 °C with a heating rate of 5 °C/min. The measurements were performed in 5%O_2/Ar gas of 200 ml/min (Volumetric percentage). During the mass spectroscopy analysis, the following desorbed species were recorded; m/z: 44 (CO_2) and 18 (H_2O). The CO_2 signal in the graph was enlarged 10 times for the analysis.

2.3. Catalytic performance tests

The catalytic tests of CO_2 methanation were performed in a fixed-bed flow reactor (inner diameter: 8 mm) under atmospheric pressure. The temperature in the catalytic bed was monitored using a K-type thermocouple, which was placed close to the catalyst bed. Before the tests, the calcined materials were reduced in situ from room temperature to 900 °C with a heating rate of 5°C/min under reduction gas (5%H_2/Ar: 100 ml/min) and kept 1 h at 900 °C. The reduction temperature was 900 °C because the nickel species could be reduced thoroughly at 900 °C according to the TPR result, which was also used in other literature [49]. After the reduction, the reactor was cooled down to 200°C and the reaction mixture was introduced with a molar ratio of Ar/H_2/CO_2=25/60/15 and the GHSV of 12,000 h^{-1}. The methanation tests were performed in the temperature range from 200 to 400 °C with a temperature

step of 50 °C, which are appropriate conditions for Ni-containing mixed oxides, as reported in many literatures [49,59]. At each plateau of temperature, the catalyst was kept for 30 min, corresponding to a steady-state measurement. The flow rates of inlet and outlet were measured by flowmeter at each temperature when the reaction was stable. And the measured flow rates and the compositions obtained from GC were used to calculate the CO_2 conversion (X_{CO2}) and CH_4 selectivity (S_{CH4}).

CO_2 conversion (X_{CO2}) and CH_4 selectivity (S_{CH4}) are defined as:

$$\textbf{Conversion of } CO_2 = X_{CO2} \quad (\%) \qquad \frac{[CO2]in-[CO2]out}{[CO2]in} = \frac{\%CO2in.Qin-\%CO2out.Qout}{\%CO2in.Qin} * 100$$

$$\textbf{Selectivity of } CH_4 = S_{CH4} \quad (\%) \qquad \frac{[CH4]out}{[CO2]in-[CO2]out} = \frac{\%CH4out.Qout}{\%CO2in.Qin-\%CO2out.Qout} * 100$$

In which Q is the flow rate ("in" for inlet, "out" for outlet).

3. Results and discussion

3.1. Characterization of the catalysts before methanation

3.1.1. Structural parameters, elemental composition, and textural properties of nano-mixed oxides derived from hydrotalcite

Structural parameters calculated from the XRD diffractograms acquired for as-synthesized materials are reported in **Table 1**. The structural parameters ***a*** and ***c*** were obtained by the equations of $a=2d_{(110)}$ and $c=d_{(003)}+2d_{(006)}+3d_{(009)}$. The crystallographic parameter ***a*** ($2d_{110}$) is associated with the average cation-cation distance in the hydroxide layers [33]. The parameter ***a*** is stable for all materials (3.06 Å), indicating the lack of possible distortions of the lattice. As stated by García-García

et al. [69], yttrium can be incorporated into layers of double-layered hydroxides, though its ionic radius is somewhat larger than that of Al and Mg (Mg^{3+}=0.86 Å, Al^{3+}=0.675 Å, Y^{3+}=1.04 Å) [44,70]. The obtained parameter ***c*** (d_{003} + $2d_{006}$+ $3d_{009}$), which refers to the triple thickness between brucite layers in hydrotalcite structure, decreased for low Y (under 2 wt.%) modified samples in comparison to the non-modified material, except for MO-4.0Y, which increased to 23.51 Å (**Table 1**). For the MO-4.0Y, some deposition of Yttrium on the external surface may be assumed. Moreover, the distance between the brucite-like layers (***c´***=***c****/3*) is in the range of 7.79-7.84 Å, showing the presence of interlayer anions, such as e.g. CO_3^{2-} (7.65 Å) and NO_3^- (8.79 Å) [71–73]. The structural parameters revealed that the yttrium loading up to 2.0 wt.% could result in the introduction of this metal into the periclase-like structure. However, the higher content of the yttrium led to the increase of the interlayer space, which was possibly linked with the deposition of the metal on the surface of the layers. This agrees with the textural properties, as the specific surface area of MO-4.0Y significantly decreased compared with that of MO-2.0Y due to their partial blockage.

The elemental composition of nano-mixed oxides obtained by calcination acquired from the XRF method is presented in **Table 1**. All samples revealed nickel content between 16 and 20 wt.%, whereas the content of yttrium was either the same (MO-0.4Y) or close to the nominal amount (MO-2.0Y and MO-4.0Y). According to Li et al. [66], Ni^{2+} can be substituted by Y^{3+}, similarly as observed in our study (**Table 1**). The calculated M^{2+}/M^{3+} atomic ratios were fairly close to those assumed during

the materials synthesis, indicating that the composition of LDHs may be easily controlled as reported before [74].

Table 1 Structural parameters (XRD), elemental composition (XRF) and textural properties (BET analysis) of yttrium modified nano-mixed oxides derived from hydrotalcite. Additionally, the nominal values are reported in brackets.

Catalyst	Structural parameters		Elemental composition of the calcined materials			Textural properties of the calcined materials		
	a [Å][a)]	c [Å][b)]	Ni [wt.%]	Y [wt.%]	M^{2+}/M^{3+} [-]	S_{BET} [m^2/g] [c)]	V_p [cm^3/g] [d)]	d_p [nm] [e)]
MO-0Y	3.06	23.45	20	-	3.6 (3.0)	120	0.6	19
MO-0.4Y	3.06	23.38	21	0.4 (0.4)	3.5 (3.0)	120	0.5	15
MO-2.0Y	3.06	23.42	18	1.8 (2.0)	3.4 (3.0)	192	0.6	14
MO-4.0Y	3.06	23.51	16	3.4 (4.0)	3.7 (3.0)	153	0.7	18

[a)] calculated from d-spacing of (110) plane; $a = 2d_{110}$

[b)] calculated from appropriate d-spacings of (003), (006) and (009) planes; $c = d_{003} + 2d_{006} + 3d_{009}$

[c)] specific surface areas calculated from the BET equation

[d)] mesopore volumes obtained from the BJH desorption calculation method

[e)] pore size distribution derived from the BJH desorption calculation method

The textural parameters obtained from the N_2 sorption isotherms for the calcined materials are listed in **Table 1**. All values agree with those previously reported in the literature [35,44,45,47,49,50,54,59,64,73]. The obtained specific surface areas ranged between 120 and 192 $m^2.g^{-1}$ and the highest area was found for the MO-2.0Y catalyst. There are no significant difference regarding to BET surface area and pore volume of Ni-containing double-layered hydroxides-derived catalyst when the loading of yttrium is low (≤0.4%) compared with Y-free sample, only the average pore size decreases as

the increase of yttrium at low loading of yttrium [44,47]. As described in the section before, the structural parameters showed that the yttrium loading up to 2.0 wt.% could result in the introduction of this metal into the periclase-like structure. However, the higher content of the yttrium increased the interlayer space, which was possibly linked with the deposition of the metal on the outer surface of the layers. This agrees with the textural properties, as the specific surface area of MO-4.0 Y significantly decreased due to their partial blockage. The volume of mesopores did not change significantly after yttrium promotion. However, pore diameters diminished for MO-0.4Y and MO-2.0Y catalysts, as compared to the non-promoted material, pointing to the formation of a higher number of smaller pores when yttrium was introduced into the brucite-like layers.

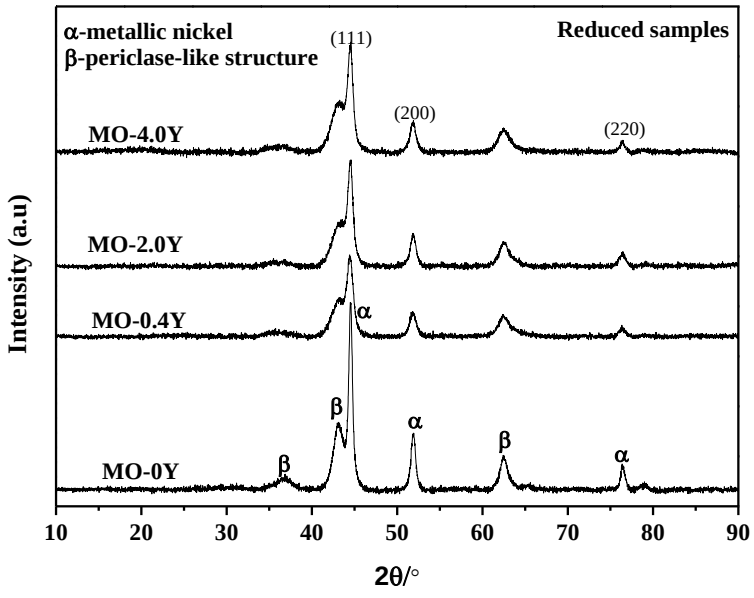

Fig. 1. XRD profiles for reduced nano-mixed oxides modified with different yttrium loadings

(0.4, 2.0, or 4.0 wt.%) and compared to the un-promoted catalyst (MO-0Y).

Fig. 1 shows XRD diffractograms of the reduced catalysts, in which metallic nickel phase (ICOD 01-087-0712) is evidenced by the presence of reflections at 2θ ca. 44.5, 53 and 76.5°, corresponding to crystal planes of (111), (200) and (220), respectively. Moreover, reflections arising from the periclase-like structure at 2θ ca. 36.7, 43 and 62.5° are observed, which corresponds to mixed oxides obtained after thermal treatment of double-layered hydroxides [44,45,47]. **Table 2** reports the size of Ni^0 crystallites, calculated from the 2θ diffraction peak at ca. 52° (corresponding to (200) crystal plane of Ni^0) using the Scherrer equation. The yttrium promotion resulted in a decrease of nickel crystallites size from ca. 13.7 nm for the parent MO to ca. 9.2 nm for MO-0.4Y. The values obtained for MO-2.0Y and MO-4.0Y catalysts were close to the one registered for the unpromoted catalyst, i.e. 12.5 and 12.3 nm, respectively.

Table 2 Ni^0 crystallite size for the reduced and spent materials calculated from XRD

Catalyst	Ni^0 crystallite size	
	Reduced samples [nm] [a)]	Spent samples [nm] [a)]
MO-0Y	13.7	9.3
MO-0.4Y	9.2	7.9
MO-2.0Y	12.5	7.6
MO-4.0Y	12.3	7.5

[a)] Calculated from the Scherrer equation at 2θ =52°

3.1.2. Reducibility of catalysts followed by H_2-TPR

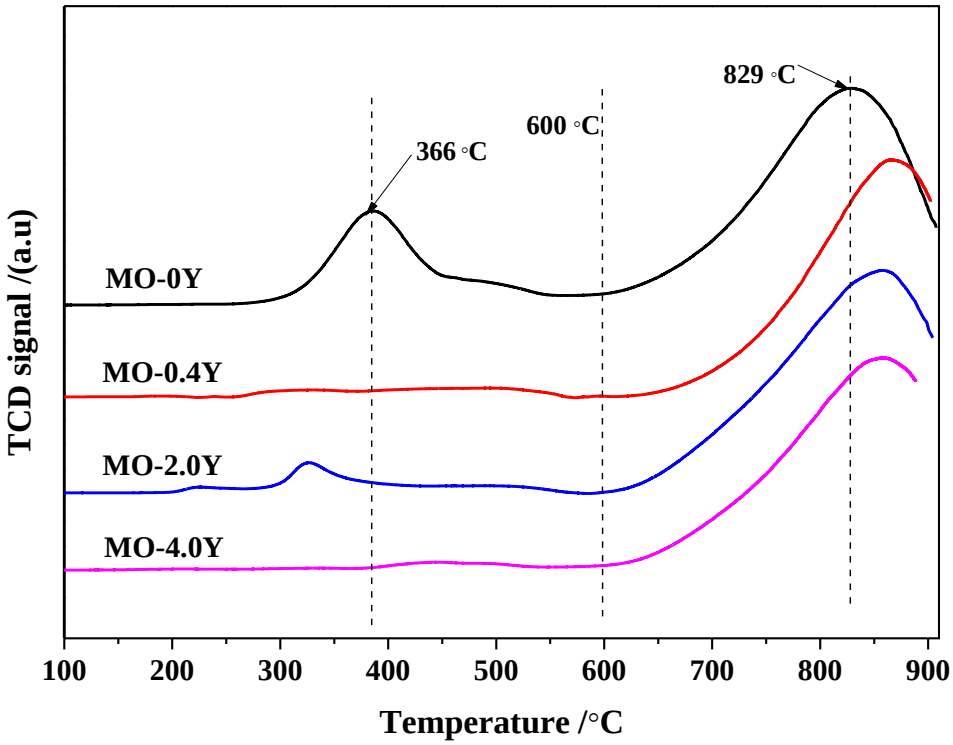

Fig. 2. H_2-TPR profiles for mixed oxides modified with different yttrium loadings (0.4, 2.0 or 4.0 wt.%) compared to the non-promoted catalyst (MO-0Y).

Fig. 2 shows the H_2-TPR of calcined mixed oxides (MO). As demonstrated in other reports, yttrium cannot be reduced under the conditions used in the measurements [66,67]. The reduction profile of MO-0Y has two main reduction bands that centered at 366 °C and 829 °C, which corresponds respectively to the reduction of nickel oxides weakly bonded with the double layered hydroxides and nickel species that are incorporated into the structure of hydroxides [31,44,63,66,67,75]. The high-temperature peak shifts towards higher temperatures for all Y-promoted catalysts (**Table 3**, 858-866 °C), which indicates stronger interaction between nickel oxide

species and the support matrix in comparison with Y-free sample [44]. For 2.0 and 4.0 wt.% of Y, the shift of latter peak was less pronounced, as shown in **Table 3**, indicating less strong metal-support interaction. This might be due to the segregation of yttrium or lattice substitution of nickel species by yttrium [66]. The reduction peaks at temperatures lower than 600 °C presented low intensity for Y-modified samples in comparison to the unpromoted catalyst (MO-0Y), which means that the loading of Y results in a decreased reducibility. This phenomenon was already observed in hydrotalcite derived mixed oxides catalysts modified by Y and Zr in CO_2 dry reforming reaction, in which the adding of Y and Zr resulted in a decrease of the reducibility of nickel [31,44]. As calculated in **Table 3**, the highest H_2 consumption (1.67 mmol) was obtained for the Y-free mixed-oxide sample. After the introduction of yttrium, the H_2 consumptions (1.15-1.38 mmol) of yttrium-promoted mixed oxides decreased in contrast to the yttrium-free sample, demonstrating decreased reducibility of NiO for yttrium-promoted mixed oxides.

Table 3 H_2 consumption according to H_2-TPR analyses

Catalyst	Temperature (°C)		H_2 consumption ($mmolH_2/g$)		
	<600	>600	<600	>600	Total
MO-0Y	386	829	0.37	1.30	1.67
MO-0.4Y	320	866	0.07	1.09	1.16
MO-2.0Y	327	858	0.11	1.27	1.38
MO-4.0Y	444	858	0.05	1.10	1.15

3.1.3. Basicity of the catalysts derived from CO_2-TPD

Fig. 3 shows the CO_2-TPD profiles of the reduced MO catalysts. Three types of CO_2 desorption peaks could be observed with a maximum temperature of 138, 203 and 364 °C for MO-0Y sample, which refers to weak, medium (intermediate) and strong basic sites, respectively [33,43,44,54]. Similar peaks were found for yttrium-promoted mixed oxides materials, with the maximum temperature of CO_2 desorption peak shifted towards lower temperature with the increasing yttrium content compared to the MO-0Y sample, indicating that the loading of Y changed the number and distribution of the basic sites. This phenomenon was also observed in other literature [44].

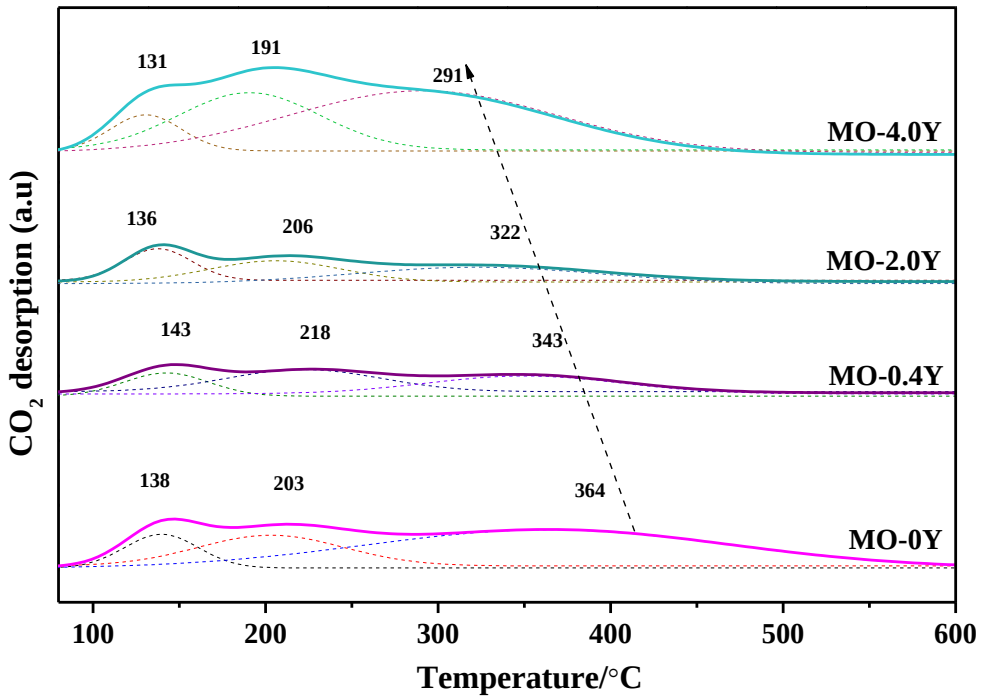

Fig. 3. CO_2-TPD profiles for mixed oxides catalysts

As calculated in **Table 4**, the amount of different type of basic sites for the

Y-modified samples increased with the increase of yttrium loading (from 0.4 to 4.0 wt%) and the total number of basic sites also increased with the increased Y content, with MO-4.0Y having the highest number of each type of basic sites as well as the total basic sites. Compared to the basicity of MO-0Y sample, the materials with 0.4 wt.% and 2.0 wt.% of Y showed lower content of total basic sites and individual type of basic sites (weak, medium or strong). But compared to that of the MO-0Y, the percentage share of weak or intermediate basic sites for MO-0.4Y and MO-2.0Y was higher, with lower content of the share of strong basic sites, meaning that the doping of yttrium significantly changed the distribution of basic sites on Y-modified samples. In conclude, the introduction of Y with low content (0.4 wt.% and 2.0 wt.%) results in the increase of share of medium basic sites as the expense of strong type. The highest share of medium-strength basic sites was found on the MO-0.4Y sample.

Table 4 Basicity of the studied catalysts, calculated from TPD-CO_2 for the reduced materials.

Catalyst	Basic sites [μmol/g]				Basic sites distribution [%]		
	Weak	Medium	Strong	Total basicity	Weak	Medium	Strong
MO-0Y	16.4	43.9	46.3	106.6	15.4	41.2	43.4
MO-0.4Y	9.4	33.7	14.6	57.7	16.2	58.5	25.3
MO-2.0Y	11.6	35.2	26.4	73.2	15.8	48.1	36.1
MO-4.0Y	41.4	91.5	91.2	224.1	18.5	40.8	40.7

3.2. Catalytic performance tests for CO_2 methanation

Fig. 4 presents the CO_2 conversion and **Fig.5** presents the methane selectivity measured during catalytic experiments for the studied mixed oxides (MO) promoted with different amounts of Y as a function of reaction temperature.

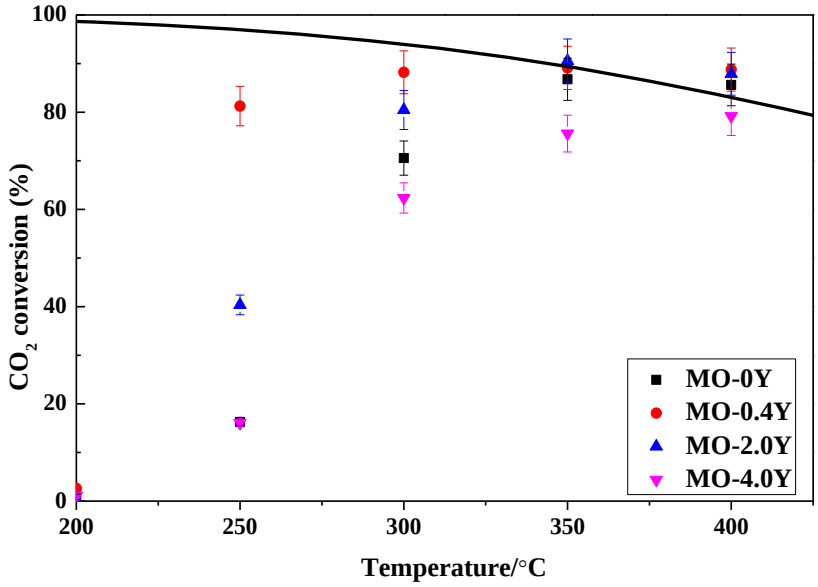

Fig. 4. CO_2 conversion of the studied mixed oxides catalysts (MO-0Y, MO-0.4Y, MO-2.0Y, MO-4.0Y). Experimental conditions of CO_2 methanation: GHSV=12000 h^{-1}, total flow 100 mL/min, $CO_2/H_2/Ar$ =15/60/25.

The thick continuous line shown in **Fig. 4** represents the thermodynamic equilibrium calculated for the conditions used in this work [33,54]. According to thermodynamics, CO_2 methanation is favored at low temperatures and it decreases with the increasing temperature due to the co-existence of parallel reactions, such as reverse water-gas shift (RWGS) or reforming [33,76]. The latter results in undesired side products, among them carbon monoxide [59]. All mixed oxides were catalytically active in CO_2 methanation. The obtained conversions at 250 °C were much lower than the thermodynamic limitations, except for the MO-0.4Y catalyst. Depending on the Y-loading a change in the catalytic performance of the catalysts was observed.

Nevertheless, the increase of the catalytic conversion was not directly correlated to the increase of yttrium loading. For both series of results registered at 250 °C and 300 °C, the sequence for the CO_2 conversion was: MO-0.4Y > MO-2.0Y > MO-0Y > MO-4.0Y. CO_2 conversion increased at 250 °C from 16% for MO-0Y to 40% and 81% for MO-2.0Y and MO-0.4Y, respectively, and at 300°C, from 71% for MO-0Y to 80% and 88% for MO-2.0Y and MO-0.4Y, respectively. At both temperatures, 250 °C and 300 °C, the selectivity towards methane was higher than 98.5%, with very low differences between the Y-promoted catalysts (**Fig.5**). However, in the tested temperature range, both the CO_2 conversion and CH_4 selectivity for MO-4.0Y decreased in comparison to MO-0Y. This could have been caused by the deposition of the yttrium on the external surface of the support matrix and the weaker metal-support interaction, as confirmed by XRD and TPR-H_2.

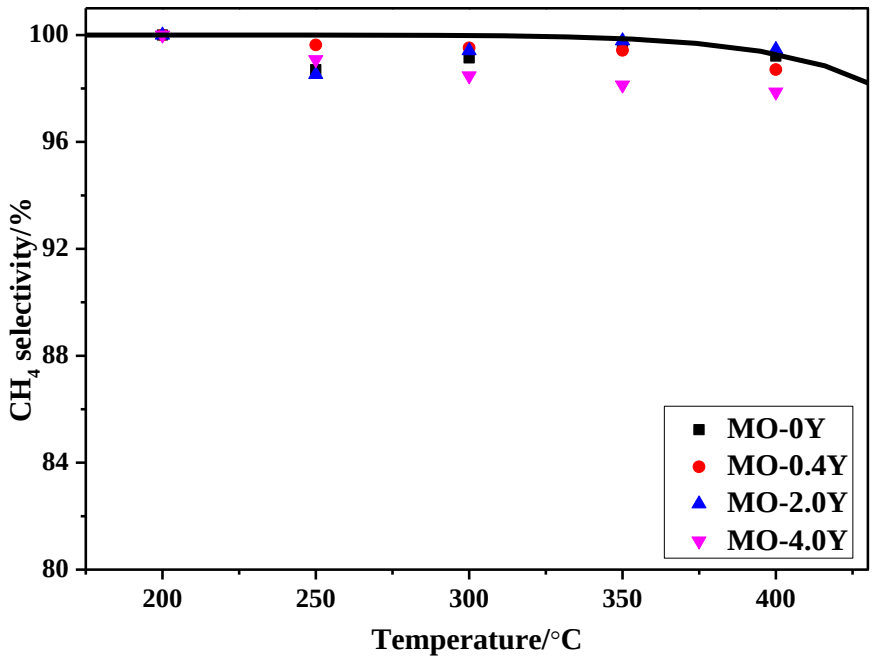

Fig. 5. CH_4 selectivity of the studied mixed oxides catalysts (MO-0Y, MO-0.4Y, MO-2.0Y,

MO-4.0Y). Experimental conditions of CO_2 methanation: GHSV = 12000 h^{-1}, total flow 100 ml/min, $CO_2/H_2/Ar$ = 15/60/25.

The enhancement of the activity of Y-promoted catalysts except MO-4.0Y can be partially explained by the smaller Ni^0 crystallite size in comparison to the non-promoted sample, which is also found for La-promoted Ni-containing hydrotalcite-derived mixed oxides in CO_2 methanation [46].

Simultaneously, the MO-0.4Y catalyst showed the highest percentage share of intermediate-strength basic sites. Pan et al. [77] claimed that Lewis acid-base sites are involved in the CO_2 methanation mechanism and the CO_2 adsorbed on strong basic sites did not participate in the reaction and the medium-strength basic sites played an important role in the reaction. In the current study, a linear correlation between CO_2 conversion and percentage share of medium-strength basic sites can be drawn at 250 °C and 300 °C (**Fig. 6**). It shows that the CO_2 conversion increase as the increase of the percentage share of medium-strength basic sites.

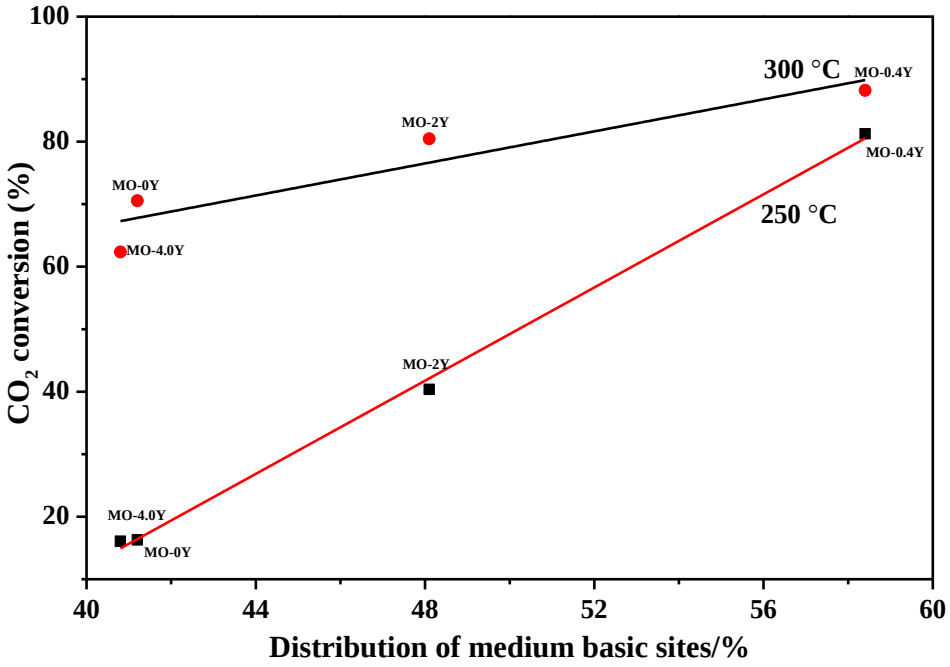

Fig. 6. CO_2 conversion at 250 °C and 300 °C versus percentage share of medium basic sites of tested catalysts, the black points represent CO_2 conversion at 250 °C and the red points represent CO_2 conversion at 300 °C

The medium-strength basic sites play a significant role in the methanation process. Wierzbicki et al. [49,59] found that there was a good linear correlation between the number of medium-strength basic sites and the CO_2 conversion on the unpromoted and La-promoted LDHs catalysts. This work confirms that the percentage of medium-strength basic sites have a considerable influence in the case of carbon dioxide methanation on Ni-containing Y-modified mixed oxides catalysts.

Besides, the TPR results show that MO-0.4Y has the highest intensity of metal-support interaction compared to that of other samples [78]. In conclude, the decreased nickel particle size, increased share of medium-strength basic sites and stronger metal-support interactions found for MO-0.4Y catalyst greatly contributed to the enhanced catalytic activity in CO_2 methanation.

3.3. Characterization of the spent catalysts

3.3.1 XRD patterns of the spent samples

Ni^0 crystallite sizes calculated for the spent catalysts are reported in **Table 2**. A decrease of the crystallite size was found for the spent catalysts compared to that of the reduced samples, in agreement with Świrk et al. [44] and Dębek et al. [31] on similar materials for other CO_2 reactions. This can be explained by the loss of crystallinity of the Ni phase due to its possible re-dispersion of nickel particles. The decreased crystallite size of Ni^0 species also indicates that no sintering happened during reaction.

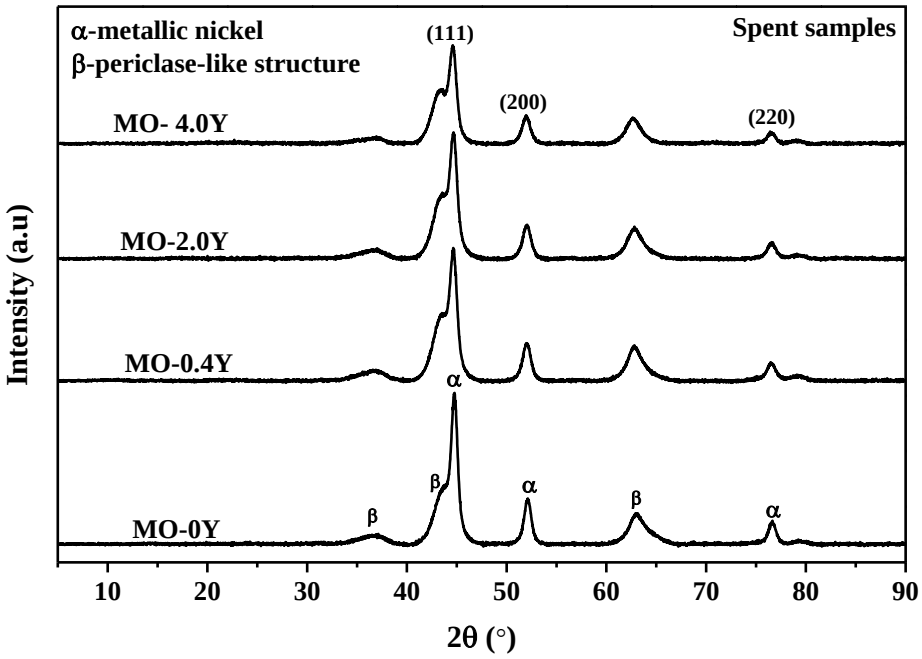

Fig. 7. XRD diffractograms of spent Y modified mixed oxides (0.4, 2.0, or 4.0 wt.%) as compared to the unpromoted catalyst (MO-0Y).

After the methanation tests, no reflections corresponding to graphitic carbon (at 2θ=27˚) were observed in the diffractograms of the spent catalysts (**Fig. 7**). Thus, extensive coking with graphite formation may be excluded. This is in agreement with

the studies of other authors e.g. Wierzbicki et al. [49], who confirmed the absence of carbon deposition on Ni/Al LDHs-like catalysts for CO_2 methanation.

3.3.2 TGA and TPO tests of the spent samples

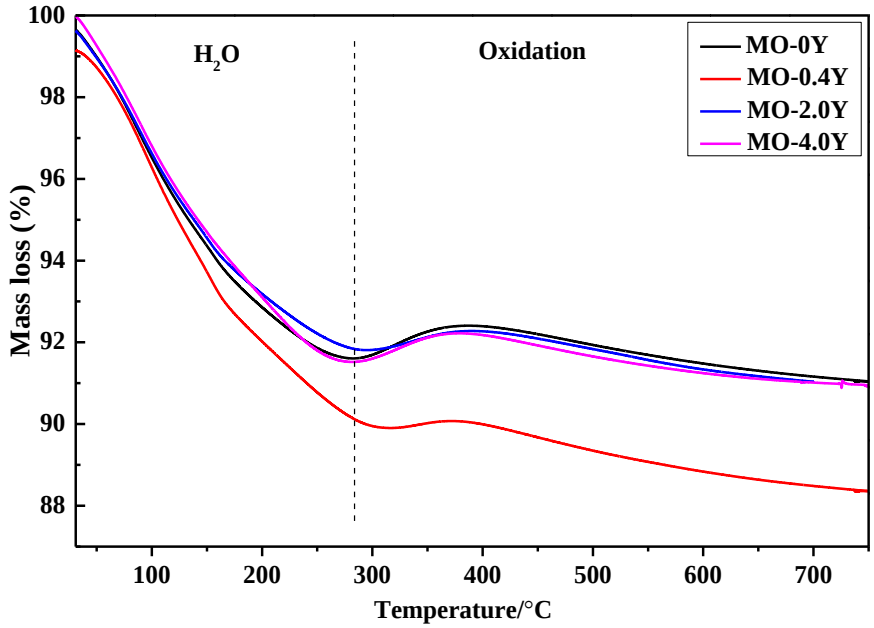

Fig. 8. TGA plots of the studied catalysts (MO-Y0, MO-Y0.4, MO-Y2.0, MO-Y4.0) tested in the methanation process.

Thermogravimetric analyses were carried out for the spent catalysts in order to verify if other non-crystalline carbon species may have been formed (**Fig. 8**). From **Fig.8**, two mass loss regions can be observed for all tested MO samples, corresponding respectively to the removal of physically adsorbed water (<250°C) and a higher temperature region (>400°C) corresponding to oxidation of metallic nickel to nickel oxide and the removal of residues. From TGA, one can conclude that no significant amount of carbonaceous species was present on the surface of the spent

catalysts. To confirm this, temperature-programmed oxidation tests were performed from RT to 650 °C on MO-0Y (**Fig. 9a**) and MO-0.4Y catalysts (**Fig. 9b**).

(a)

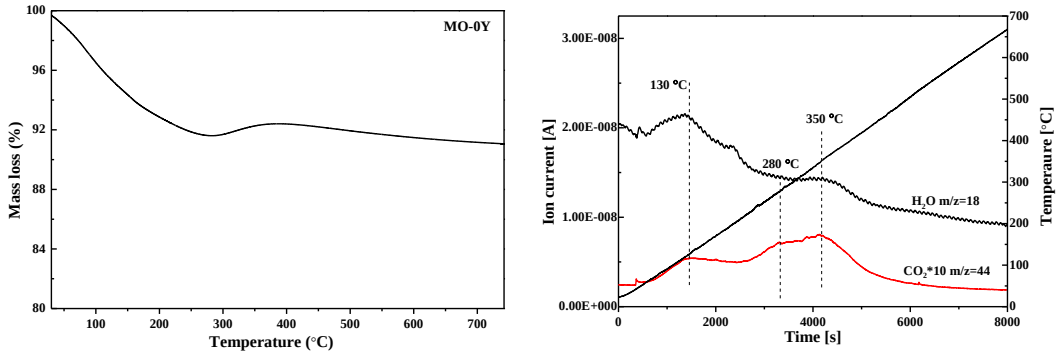

(b)

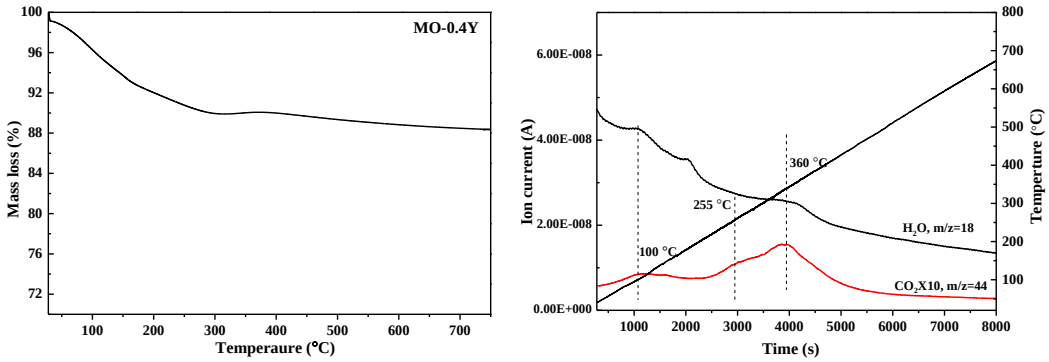

Fig. 9. Temperature-Programmed Oxidation results followed by mass spectroscopy (H_2O m/z=18 and CO_2 m/z=44x10) on catalysts; a) unpromoted MO catalysts, b) MO-0.4Y.

From **Fig.9**a and b, one can observe that CO_2 formation corresponding to the decomposition of carbonaceous species (250-500°C) is very low, confirming

insignificant amounts of the formed carbonaceous species during the CO_2 methanation reaction on the Y promoted catalysts. Thus, the main byproduct in the reaction is CO.

4. Conclusions

Yttrium-promoted Ni/Mg/Al hydrotalcite-derived catalysts were synthesized using the co-precipitation method at constant pH. Then, the catalysts were characterized by low-temperature N_2 sorption, X-ray diffraction, elemental analysis, and temperature-programmed reduction/desorption (H_2-TPR and CO_2-TPD), and tested as catalysts in CO_2 methanation at GHSV =12000 h^{-1} using a mixture of $CO_2/H_2/Ar$ =15/60/25.

The addition of Y affected the CO_2 adsorption capacity of the materials by changing the distribution of the basic sites, especially those of medium-strength. As proven by H_2-TPR, the yttrium promotion influenced the nickel/support interaction. After the introduction of yttrium, a shift of reduction peak towards higher temperatures was observed, which was attributed to the segregation of Y on the support. The Y addition affected strongly the catalytic activity in CO_2 methanation, increasing the CO_2 conversion at 250 °C from 16% for MO-0Y to 40 and 81% for MO-2.0Y and MO-0.4Y, respectively. This could be explained by both increased distribution of medium-strength basic sites and significantly smaller metallic nickel particle size of Y-promoted catalysts. Additionally, the metallic nickel crystallite size decreased after the reaction, which points to the reorganization of Ni at the surface of

the support, which could contribute to the increase of the catalytic activity in the moderate temperature region. The selectivity towards methane formation was found around 98 to 99% at 250°C. It is worth noting that the only products of the reaction registered were H_2O, CH_4 and CO. The XRD, TGA, and TPO analyses confirmed only traces of carbon in the spent catalysts.

Acknowledgments

Chao Sun would like to express his gratitude for the financial support of CSC (China Scholarship Council) for his Ph.D. research in Sorbonne Université. Katarzyna Świrk would like to acknowledge Prof. Magnus Rønning for the possibility to carry out the elemental analysis and low-temperature N_2 sorption at NTNU in Trondheim. Prof. Konrad Świerczek and Anna Olszewska are gratefully acknowledged for thermogravimetric analysis performed at AGH in Cracow.

Reference

[1] Aresta M, Dibenedetto A, Angelini A. Catalysis for the valorization of exhaust carbon: From CO2 to chemicals, materials, and fuels. technological use of CO_2. Chem Rev 2014;114:1709–42. doi:10.1021/cr4002758.

[2] Wang W, Gong J. Methanation of carbon dioxide: An overview. Front. Chem. Sci. Eng. 2011;5:2–10. doi:10.1007/s11705-010-0528-3.

[3] Guilera J, Del Valle J, Alarcón A, Díaz JA, Andreu T. Metal-oxide promoted Ni/Al_2O_3 as CO_2 methanation micro-size catalysts. J CO2 Util 2019;30:11–7. doi:10.1016/j.jcou.2019.01.003.

[4] Götz M, Lefebvre J, Mörs F, McDaniel Koch A, Graf F, Bajohr S, et al. Renewable Power-to-Gas: A technological and economic review. Renew Energy 2016;85:1371–90. doi:10.1016/j.renene.2015.07.066.

[5] Zağli E, Falconer JL. Carbon dioxide adsorption and methanation on Ruthenium. J Catal 1981;69:1–8.

[6] Li M, Amari H, van Veen AC. Metal-oxide interaction enhanced CO_2 activation

in methanation over ceria supported nickel nanocrystallites. Appl Catal B Environ 2018;239:27–35. doi:10.1016/j.apcatb.2018.07.074.

[7] Aziz MAA, Jalil AA, Triwahyono S, Ahmad A. CO_2 methanation over heterogeneous catalysts: Recent progress and future prospects. Green Chem 2015;17:2647–63. doi:10.1039/c5gc00119f.

[8] Zhang W, Yang S, Li J, Gao W, Deng Y, Dong W, et al. Visible-to-ultraviolet Upconvertion: Energy transfer, material matrix, and synthesis strategies. Appl Catal B Environ 2017;206:89–103. doi:10.1016/j.apcatb.2017.01.023.

[9] Zhen W, Gao F, Tian B, Ding P, Deng Y, Li Z, et al. Enhancing activity for carbon dioxide methanation by encapsulating (1 1 1) facet Ni particle in metal–organic frameworks at low temperature. J Catal 2017;348:200–11. doi:10.1016/j.jcat.2017.02.031.

[10] Panagiotopoulou P, Kondarides DI, Verykios XE. Selective methanation of CO over supported noble metal catalysts: Effects of the nature of the metallic phase on catalytic performance. Appl Catal A Gen 2008;344:45–54.

[11] Yaccato K, Carhart R, Hagemeyer A, Lesik A, Strasser P, Volpe AF, et al. Competitive CO and CO_2 methanation over supported noble metal catalysts in high throughput scanning mass spectrometer. Appl Catal A Gen 2005;296:30–48. doi:10.1016/j.apcata.2005.07.052.

[12] Frontera P, Macario A, Ferraro M, Antonucci P. Supported Catalysts for CO_2 Methanation: A Review. Catalysts 2017;7:59. doi:10.3390/catal7020059.

[13] Kruatim J, Jantasee S, Jongsomjit B. Improvement of cobalt dispersion on Co/SBA-15 and Co/SBA-16 catalysts by ultrasound and vacuum treatments during Post-impregnation step. Eng J 2017;21:17–28. doi:10.4186/ej.2017.21.1.17.

[14] Czuma N, Zarębska K, Motak M, Gálvez ME, Da Costa P. Ni/zeolite X derived from fly ash as catalysts for CO_2 methanation. Fuel 2020;267. doi:10.1016/j.fuel.2020.117139.

[15] Tada S, Ochieng OJ, Kikuchi R, Haneda T, Kameyama H. Promotion of CO_2 methanation activity and CH_4 selectivity at low temperatures over $Ru/CeO_2/Al_2O_3$ catalysts. Int J Hydrogen Energy 2014;39:10090–100. doi:10.1016/j.ijhydene.2014.04.133.

[16] Liu Q, Bian B, Fan J, Yang J. Cobalt doped Ni based ordered mesoporous catalysts for CO_2 methanation with enhanced catalytic performance. Int J Hydrogen Energy 2018;43:4893–901. doi:10.1016/j.ijhydene.2018.01.132.

[17] Liang C, Hu X, Wei T, Jia P, Zhang Z. Methanation of CO_2 over Ni $/Al_2O_3$ modified with alkaline earth metals : Impacts of oxygen vacancies on catalytic activity. Int J Hydrogen Energy 2019;44:8197–213. doi:10.1016/j.ijhydene.2019.02.014.

[18] Fatah NAA, Jalil AA, Rahman AFA, Hambali HU, Hussain I. CO_2 Methanation over Mesoporous Silica Based Catalyst : A Comprehensive Study. J Energy Saf Technol 2019;02:49–53.

[19] Beuls A, Swalus C, Jacquemin M, Heyen G, Karelovic A, Ruiz P. Methanation of CO2 : Further insight into the mechanism over Rh /γ-Al_2O_3 catalyst. Appl

Catal B Environ 2012;113–114:2–10. doi:10.1016/j.apcatb.2011.02.033.
[20] Shin HH, Lu L, Yang Z, Kiely CJ, McIntosh S. Cobalt Catalysts Decorated with Platinum Atoms Supported on Barium Zirconate Provide Enhanced Activity and Selectivity for CO_2 Methanation. ACS Catal 2016;6:2811–8. doi:10.1021/acscatal.6b00005.
[21] Beaumont SK, Alayoglu S, Specht C, Michalak WD, Pushkarev V V., Guo J, et al. Combining in situ NEXAFS spectroscopy and CO_2 methanation kinetics to study Pt and Co nanoparticle catalysts reveals key insights into the role of platinum in promoted cobalt catalysis. J Am Chem Soc 2014;136:9898–901. doi:10.1021/ja505286j.
[22] Panagiotopoulou P. Hydrogenation of CO_2 over supported noble metal catalysts. Appl Catal A Gen 2017;542:63–70.
[23] Ignacio Iglesias, Adrian Quindimil, Fernando Marino, Unai De-La-Torre JRG-V. Zr promotion effect in CO_2 methanation over ceria supported nickel catalysts. Int J Hydrogen Energy 2019;44:1710–9. doi:10.1016/j.ijhydene.2018.11.059.
[24] Vrijburg WL, Garbarino G, Chen W, Parastaev A, Longo A, Pidko EA, et al. Ni-Mn catalysts on silica-modified alumina for CO_2 methanation. J Catal 2020;382:358–71. doi:10.1016/j.jcat.2019.12.026.
[25] Yatagai K, Shishido Y, Gemma R, Boll T, Uchida HH, Oguri K. Mechanochemical CO_2 methanation over LaNi-based alloys. Int J Hydrogen Energy 2020;45:5264–75. doi:10.1016/j.ijhydene.2019.07.055.
[26] Everett OE, Zonetti PC, Alves OC, de Avillez RR, Appel LG. The role of oxygen vacancies in the CO_2 methanation employing Ni/ZrO_2 doped with Ca. Int J Hydrogen Energy 2020;45:6352–9. doi:10.1016/j.ijhydene.2019.12.140.
[27] Zhang T, Liu Q. Mesostructured cellular foam silica supported bimetallic $LaNi_{1-x}Co_xO_3$ catalyst for CO_2 methanation. Int J Hydrogen Energy 2020;45:4417–26. doi:10.1016/j.ijhydene.2019.12.006.
[28] Liang C, Tian H, Gao G, Zhang S, Liu Q, Dong D, et al. Methanation of CO_2 over alumina supported nickel or cobalt catalysts: Effects of the coordination between metal and support on formation of the reaction intermediates. Int J Hydrogen Energy 2020;45:531–43. doi:10.1016/j.ijhydene.2019.10.195.
[29] F. Cavani, F. Trifirò AV. Hydrotalcite-type anionic clays: Preparation, properties and applications. Catal Today 1991;11:173–301.
[30] Liu J, Bing W, Xue X, Wang F, Wang B, He S, et al. Alkaline-assisted Ni nanocatalysts with largely enhanced low-temperature activity toward CO_2 methanation. Catal Sci Technol 2016;6:3976–83. doi:10.1039/c5cy02026c.
[31] Dębek R, Motak M, Galvez ME, Grzybek T, Da Costa P. Promotion effect of zirconia on Mg(Ni,Al)O mixed oxides derived from hydrotalcites in CO_2 methane reforming. Appl Catal B Environ 2018;223:36–46. doi:10.1016/j.apcatb.2017.06.024.
[32] Dębek R, Motak M, Galvez ME, Grzybek T, Da Costa P. Influence of Ce/Zr molar ratio on catalytic performance of hydrotalcite-derived catalysts at low temperature CO_2 methane reforming. Int J Hydrogen Energy

2017;42:23556–67. doi:10.1016/j.ijhydene.2016.12.121.
[33] Liu H, Wierzbicki D, Debek R, Motak M, Grzybek T, Da Costa P, et al. La-promoted Ni-hydrotalcite-derived catalysts for dry reforming of methane at low temperatures. Fuel 2016;182:8–16. doi:10.1016/j.fuel.2016.05.073.
[34] Dębek R, Radlik M, Motak M, Galvez ME, Turek W, Da Costa P, et al. Ni-containing Ce-promoted hydrotalcite derived materials as catalysts for methane reforming with carbon dioxide at low temperature - On the effect of basicity. Catal Today 2015;257:59–65. doi:10.1016/j.cattod.2015.03.017.
[35] Wierzbicki D, Dębek R, Szczurowski J, Basąg S, Włodarczyk M, Motak M, et al. Copper, cobalt and manganese: Modified hydrotalcite materials as catalysts for the selective catalytic reduction of NO with ammonia. the influence of manganese concentration. Comptes Rendus Chim 2015;18:1074–83.
[36] Chmielarz L, Kuśtrowski P, Rafalska-Łasocha A, Majda D, Dziembaj R. Catalytic activity of Co-Mg-Al, Cu-Mg-Al and Cu-Co-Mg-Al mixed oxides derived from hydrotalcites in SCR of NO with ammonia. Appl Catal B Environ 2002;35:195–210. doi:10.1016/S0926-3373(01)00254-5.
[37] Carja G, Delahay G. Mesoporous mixed oxides derived from pillared oxovanadates layered double hydroxides as new catalysts for the selective catalytic reduction of NO by NH_3. Appl Catal B Environ 2004;47:59–66. doi:10.1016/j.apcatb.2003.07.004.
[38] Wu X, Feng Y, Du Y, Liu X, Zou C, Li Z. Enhancing DeNOx performance of CoMnAl mixed metal oxides in low-temperature NH_3-SCR by optimizing layered double hydroxides (LDHs) precursor template. Appl Surf Sci 2019;467–468:802–10. doi:10.1016/j.apsusc.2018.10.191.
[39] Quoc TT, Du SL, Van DP, Khac NN, Dinh LT. Temporary overvoltages in the Vietnam 500 kV transmission line. Proc IEEE Int Conf Transm Distrib Constr Live Line Maintenance, ESMO 1998:225–30. doi:10.1109/tdcllm.1998.668378.
[40] Chai R, Fan S, Zhang Z, Chen P, Zhao G, Liu Y, et al. Free-Standing NiO-MgO-Al_2O_3 Nanosheets Derived from Layered Double Hydroxides Grown onto FeCrAl-Fiber as Structured Catalysts for Dry Reforming of Methane. ACS Sustain Chem Eng 2017;5:4517–22. doi:10.1021/acssuschemeng.7b00717.
[41] Zhang X, Yang C, Zhang Y, Xu Y, Shang S, Yin Y. Ni-Co catalyst derived from layered double hydroxides for dry reforming of methane. Int J Hydrogen Energy 2015;40:16115–26. doi:10.1016/j.ijhydene.2015.09.150.
[42] Tsyganok AI, Tsunoda T, Hamakawa S, Suzuki K, Takehira K, Hayakawa T. Dry reforming of methane over catalysts derived from nickel-containing Mg-Al layered double hydroxides. J Catal 2003;213:191–203. doi:10.1016/S0021-9517(02)00047-7.
[43] Dębek R, Radlik M, Motak M, Galvez ME, Turek W, Da Costa P, et al. Ni-containing Ce-promoted hydrotalcite derived materials as catalysts for methane reforming with carbon dioxide at low temperature - On the effect of basicity. Catal Today 2015;257:59–65. doi:10.1016/j.cattod.2015.03.017.

[44] Świrk K, Gálvez ME, Motak M, Grzybek T, Rønning M, Da Costa P. Yttrium promoted Ni-based double-layered hydroxides for dry methane reforming. J CO2 Util 2018;27:247–58. doi:10.1016/j.jcou.2018.08.004.

[45] Świrk K, Gálvez ME, Motak M, Grzybek T, Rønning M, Da Costa P. Dry reforming of methane over Zr- and Y-modified Ni/Mg/Al double-layered hydroxides. Catal Commun 2018;117:26–32.

[46] Wierzbicki D, Motak M, Grzybek T, Gálvez ME, Da Costa P. The influence of lanthanum incorporation method on the performance of nickel-containing hydrotalcite-derived catalysts in CO_2 methanation reaction. Catal Today 2018;307:205–11. doi:10.1016/j.cattod.2017.04.020.

[47] Świrk K, Motak M, Grzybek T, Rønning M, Da Costa P. Effect of low loading of yttrium on Ni-based layered double hydroxides in CO_2 reforming of CH_4. React Kinet Mech Catal 2018. doi:10.1007/s11144-018-1515-9.

[48] Wierzbicki D, Baran R, Dębek R, Motak M, Gálvez ME, Grzybek T, et al. Examination of the influence of La promotion on Ni state in hydrotalcite-derived catalysts under CO_2 methanation reaction conditions: Operando X-ray absorption and emission spectroscopy investigation. Appl Catal B Environ 2018;232:409–19. doi:10.1016/j.apcatb.2018.03.089.

[49] Wierzbicki D, Baran R, Dębek R, Motak M, Grzybek T, Gálvez ME, et al. The influence of nickel content on the performance of hydrotalcite-derived catalysts in CO_2 methanation reaction. Int J Hydrogen Energy 2017;42:23548–55. doi:10.1016/j.ijhydene.2017.02.148.

[50] Wierzbicki D, Debek R, Motak M, Grzybek T, Gálvez ME, Da Costa P. Novel Ni-La-hydrotalcite derived catalysts for CO_2 methanation. Catal Commun 2016;83:5–8. doi:10.1016/j.catcom.2016.04.021.

[51] Wierzbicki D, Moreno MV, Ognier S, Motak M, Grzybek T, Da Costa P, et al. Ni-Fe layered double hydroxide derived catalysts for non-plasma and DBD plasma-assisted CO_2 methanation. Int J Hydrogen Energy 2019. doi:10.1016/j.ijhydene.2019.06.095.

[52] Zhang Z, Tian Y, Zhang L, Hu S, Xiang J, Wang Y, et al. Impacts of nickel loading on properties, catalytic behaviors of Ni/γ–Al_2O_3 catalysts and the reaction intermediates formed in methanation of CO2. Int J Hydrogen Energy 2019;44:9291–306. doi:10.1016/j.ijhydene.2019.02.129.

[53] Zhou J, Ma H, Liu C, Zhang H, Ying W. High temperature methanation over Ni catalysts supported on high surface area $ZnxMg_{1-x}Al_2O_4$: Influence on Zn loading. Int J Hydrogen Energy 2019;44:13253–61. doi:10.1016/j.ijhydene.2019.03.197.

[54] Wierzbicki D, Baran R, Dębek R, Motak M, Gálvez ME, Grzybek T, et al. Examination of the influence of La promotion on Ni state in hydrotalcite-derived catalysts under CO_2 methanation reaction conditions: Operando X-ray absorption and emission spectroscopy investigation. Appl Catal B Environ 2018;232:409–19. doi:10.1016/j.apcatb.2018.03.089.

[55] Wang X, Zhen T, Yu C. Application of Ni–Al-hydrotalcite-derived catalyst modified with Fe or Mg in CO_2 methanation. Appl Petrochemical Res

2016;6:217–23.
[56] Fan Z, Sun K, Rui N, Zhao B, Liu CJ. Improved activity of $Ni/MgAl_2O_4$ for CO2 methanation by the plasma decomposition. J Energy Chem 2015;24:655–9.
[57] Fan Z, Sun K, Rui N, Zhao B, Liu CJ. Improved activity of $Ni/MgAl_2O_4$ for CO_2 methanation by the plasma decomposition. J Energy Chem 2015;24:655–9. doi:10.1016/j.jechem.2015.09.004.
[58] Mebrahtu C, Krebs F, Perathoner S, Abate S, Centi G, Palkovits R. Hydrotalcite based Ni-Fe/$(Mg,Al)O_x$ catalysts for CO_2 methanation-tailoring Fe content for improved CO dissociation, basicity, and particle size. Catal Sci Technol 2018;8:1016–27.
[59] Wierzbicki D, Motak M, Grzybek T, Gálvez ME, Da Costa P. The influence of lanthanum incorporation method on the performance of nickel-containing hydrotalcite-derived catalysts in CO_2 methanation reaction. Catal Today 2018;307:205–11.
[60] Pan Q, Peng J, Sun T, Wang S, Wang S. Insight into the reaction route of CO_2 methanation: Promotion effect of medium basic sites. Catal Commun 2014;45:74–8. doi:10.1016/j.catcom.2013.10.034.
[61] J. M. Ferna´ndez, C. Barriga, M. A. Ulibarri, F. M. Labajos and V. Rives. New Hydrotalcite-like Compounds Containing Yttrium. Chem Mater 1997, 1997;9:312–8.
[62] Liu HR, Świrk K, Galvez ME, da Costa P. Nickel Supported Modified Ceria Zirconia Lanthanum/ Praseodymium/Yttrium Oxides Catalysts for Syngas Production through Dry Methane Reforming. Mater Sci Forum 2018;941:2214–9. doi:10.4028/www.scientific.net/msf.941.2214.
[63] Świrk K, Gálvez ME, Motak M, Grzybek T, Rønning M, Da Costa P. Syngas production from dry methane reforming over yttrium-promoted nickel-KIT-6 catalysts. Int J Hydrogen Energy 2018:1–13. doi:10.1016/j.ijhydene.2018.02.164.
[64] Świrk K, Rønning M, Motak M, Beaunier P, Da Costa P, Grzybek T. Ce- and Y-Modified Double-Layered Hydroxides as Catalysts for Dry Reforming of Methane: On the Effect of Yttrium Promotion. Catalysts 2019;9:56. doi:10.3390/catal9010056.
[65] Świrk K, Gálvez ME, Motak M, Grzybek T, Rønning M, Da Costa P. Dry reforming of methane over Zr- and Y-modified Ni/Mg/Al double-layered hydroxides. Catal Commun 2018;117:26–32. doi:10.1016/j.catcom.2018.08.024.
[66] Li JF, Xia C, Au CT, Liu BS. Y_2O_3-promoted NiO/SBA-15 catalysts highly active for CO2/CH4 reforming. Int J Hydrogen Energy 2014;39:10927–40. doi:10.1016/j.ijhydene.2014.05.021.
[67] Bellido JDA, Assaf EM. Effect of the Y_2O_3-ZrO_2 support composition on nickel catalyst evaluated in dry reforming of methane. Appl Catal A Gen 2009;352:179–87.
[68] Muroyama H, Tsuda Y, Asakoshi T, Masitah H, Okanishi T, Matsui T, et al.

Carbon dioxide methanation over Ni catalysts supported on various metal oxides. J Catal 2016;343:178–84.

[69] García-García JM, Pérez-Bernal ME, Ruano-Casero RJ, Rives V. Chromium and yttrium-doped magnesium aluminum oxides prepared from layered double hydroxides. Solid State Sci 2007;9:1115–25. doi:10.1016/j.solidstatesciences.2007.07.029.

[70] Fernández JM, Barriga C, Ulibarri MA, Labajos FM, Rives V. New Hydrotalcite-like Compounds Containing Yttrium. Chem Mater 1997;9:312–8. doi:10.1021/cm9603720.

[71] Kovanda F, Koloušek D, Cílová Z, Hulínský V. Crystallization of synthetic hydrotalcite under hydrothermal conditions. Appl Clay Sci 2005;28:101–9. doi:10.1016/j.clay.2004.01.009.

[72] Kloprogge JT, Kristóf J, Frost RL. Thermogravimetric analysis-mass spectrometry (TGA-MS) of hydrotalcites containing CO_3^{2-}, NO_3^-, Cl^-, SO_4^{2-} or ClO_4^-. 2003.

[73] Cavani F, Trifirò F, Vaccari A. Hydrotalcite-type anionic clays: Preparation, properties and applications. Catal Today 1991;11:173–301. doi:10.1016/0920-5861(91)80068-K.

[74] Dębek R, Galvez ME, Launay F, Motak M, Grzybek T, Da Costa P. Low temperature dry methane reforming over Ce, Zr and CeZr promoted Ni–Mg–Al hydrotalcite-derived catalysts. Int J Hydrogen Energy 2016;41:11616–23. doi:10.1016/j.ijhydene.2016.02.074.

[75] Sánchez EA, D'Angelo MA, Comelli RA. Hydrogen production from glycerol on Ni/Al_2O_3 catalyst. Int J Hydrogen Energy 2010;35:5902–7. doi:10.1016/j.ijhydene.2009.12.115.

[76] Wang L, Liu H, Liu Y, Chen Y, Yang S. Effect of precipitants on $Ni\text{-}CeO_2$ catalysts prepared by a co-precipitation method for the reverse water-gas shift reaction. J Rare Earths 2013;31:969–74. doi:10.1016/S1002-0721(13)60014-9.

[77] Wang S, Pan Q, Peng J, Sun T, Gao D, Wang S. CO_2 methanation on $Ni/Ce_{0.5}Zr_{0.5}O_2$ catalysts for the production of synthetic natural gas. Fuel Process Technol 2014;123:166–71. doi:10.1016/j.fuproc.2014.01.004.

[78] Kumar R, Kumar K, Pant KK, Choudary N V. Tuning the metal-support interaction of methane tri-reforming catalysts for industrial flue gas utilization. Int J Hydrogen Energy 2019;45:1911–29. doi:10.1016/j.ijhydene.2019.11.111.